Nonlinear Dyn (2024) 112:9419–9430
https://doi.org/10.1007/s11071-024-09549-0

ORIGINAL PAPER

Propagation dynamics of multipole solitons generated in complex fractional Ginzburg–Landau systems

Jianjun Wen · Haowen Wang · Yan Xiao

Received: 13 September 2023 / Accepted: 14 March 2024 / Published online: 15 April 2024

Abstract Based on the complex Ginzburg–Landau equation, propagation dynamics of multipole solitons generated in the dissipative system are numerically investigated by the split-step Fourier method. The effect of the value of the different Lévy indexes on stability regions of the soliton has been explored. In addition, we observe domains of different outcomes of the evolution of the input beam in the parameter plane of linear loss coefficient or diffraction gain coefficient and cubic gain coefficient. The results show that the evolution can lead to three different outcomes: decay, development into stable single soliton, expansion into the spreading pattern. We also study the evolution of multipole solitons generated with larger quintic loss coefficients and find that the input splits into the symmetrical fragments in the initial propagation. It is also demonstrated that two solitons or three solitons merge into the single soliton. Meanwhile, the relationship of merging distance with Lévy index and initial amplitude is also given.

Keywords Complex Ginzburg–Landau equation · Pearcey–Gaussian beam · Multipole solitons

J. Wen · H. Wang · Y. Xiao (✉)
College of Physics and Electronics Engineering, Shanxi University, Taiyuan 030006, China
e-mail: xiaoyan@sxu.edu.cn

1 Introduction

In the past few decades, optical solitons have been studied extensively because of their broad application prospects in the field of optical communication [1, 2]. As early as 1973, the single soliton solution and the n-order soliton solution of the nonlinear Schrödinger equation were obtained via the inverse scattering transformation method by Hasegawa and Tappert, thus theoretically predicting the formation of solitons in optical fibers [3]. Subsequently, in 1980, Mollenauer et al. at Bell Laboratories experimentally succeeded in observing the transport of the soliton in optical fibers, which verified the inference of Hasegawa and Tappert [4]. However, in practical applications, the long-distance and high-speed optical fiber communication system also contained the supply of energy and the balance between losses during transmission. Therefore, the dissipative solitons in the dissipative system have received a lot of attention from researchers in recent years. The concept of dissipative system was initially proposed in the thermodynamic system, which refers to an open system far away from the equilibrium state. Through constantly exchanging materials and energy with the outside world, it is possible to transit from the original disordered state to the ordered state in time and space when the changes in internal and external conditions reach a certain equilibrium state [5–7]. The introduction of the concept of dissipative systems has provided new concepts and methods for the study of the field of optics. It is worth mentioning that researchers have deeply investigated the existence and stability of dissipative solitons in dissipative nonlinear systems as well as the interaction between dissipative solitons [8–10]. It has a wide range of application prospects in the fields of pattern recognition, parallel data processing, optical fiber communication systems, all-optical switching, logic gates and laser cooling [11].

The general model of light propagation in nonlinear dissipative media is the CGLE, which can be regarded as a dissipative extension of the nonlinear Schrödinger equation and can be used to describe nonlinear dissipation phenomena such as superconductivity, fluid dynamics, the formation of reaction–diffusion modes, Bose–Einstein condensation, liquid crystals, quantum field theory, second-order phase transitions, etc. [12, 13]. In particular, the CGLE, as a realistic dynamical model of laser cavities, can be directly realized in nonlinear optics, and can support the formation of stable vortex solitons and rotating solitons [14, 15]. Subsequently, the researcher studied the interaction between solitons in the dissipative system described by the cubic–quintic competitive nonlinear Ginzburg–Landau equation. The phenomenon of fusion, repulsion, scattering and splitting among solitons has been observed [16]. Weitzner and Zaslavsky derived the fractional generalization of CGLE from the variational Euler–Lagrange equations in fractal media [17, 18]. Due to the generality of the cubic–quintic CGLE and its important role in various optical systems, numerous researchers have taken a keen interest in it, resulting in many research results. For example, localized numerical impulse solutions in diffuse neural networks modeled by the CGLE were explored in 2016 [19]. New optical solutions of CGLE arising in semiconductor lasers were explored in 2019 [20]. In 2020, researchers used the fractional Riccati method and the fractional bifunction method to solve a $(2 + 1)$-dimensional CGLE, and analyzed the exact traveling wave solutions including soliton solutions and combined soliton solutions [21]. The exact solutions of the CGLE in the sense of the conformable fractional derivative were established via the complete discrimination system method in 2021 [22].

Optical solitons in complex Ginzburg–Landau dissipative systems with fractional diffraction have been extensively studied in recent years, and it has been found that many novel physical phenomena of optical solitons have been obtained. In 2018, the transport characteristics and stability conditions of the dark, bright, combined dark-bright, singular, combined singular optical solitons formed by fractional diffraction Ginzburg–Landau system were investigated in Kerr media [23]. The soliton solutions of CGLE were constructed in Kerr and non-Kerr media in 2018. These new solitons were optical solitons in dissipative space described by hyperbolic functions, trigonometric functions and rational functions [24]. Using the improved Jacobian elliptic function expansion method, the researcher derived discrete soliton solutions of conformable fractional discrete CGLE in 2021 [25]. In order to further discuss the kinetic behavior of the Ginzburg–Landau equation for fractional diffraction, the researchers acquired the trigonometric, hyperbolic trigonometric and rational solutions through the improved F-expansion method in the sense of quadratic-cubic nonlinearity, and obtained the bright, dark, combined bright-dark, singular soliton, mixed singular soliton and singular periodic wave solutions in 2023 [26].

In the recent period, due to the novel properties and potential application value of Pearcey–Gaussian beam, it has been widely studied by researchers, which has produced a lot of new research results, such as tightly focused characteristics of the auto-focusing linear polarized circular Pearcey–Gaussian vortex beams (CPeGVBs) with on-axis and off-axis vortex pairs through high numerical aperture that were reported in 2021. The results had the wide applications in reverse shaping of focal fields and optical trapping control [27]. The evolution and interaction of the Pearcey–Gaussian beam in nonlinear Kerr medium were numerically studied by Lu Li et al. in 2022. The results showed that the main lobe and side lobes of Pearcey–Gaussian beam separate, forming solitons during propagation [28]. The evolution of the chirped elliptical Pearcey–Gaussian vortex (CEPGV) beams in free space was numerically investigated in 2022. It was concluded that the focusing intensity, the focal length and the transverse intensity distribution of CEPGV beams during the propagation can be controlled [29].

In the previous work, He’s team chose the Gaussian beam as the input beam. Dissipative soliton dynamics in complex fractional Ginzburg–Landau systems were studied [30]. In this paper, the Pearcey–Gaussian beam is selected as the most suitable input beam. The main reason is that on the one hand, Pearcey–Gaussian beam is a special diffractive beam, and the Pearcey–Gaussian beam, as a kind of beam similar to Airy beam, also has the characteristics of self-healing, self-accelerating and self-focusing. On the other hand, we found that Pearcey–Gaussian beams can produce good and interesting phenomena. In this paper, the propagation dynamics of Pearcey–Gaussian beams in the CGLE is numerically investigated. The results show that the dissipative single solitons and dissipative multipole solitons are obtained by the simultaneous balance of gain versus loss, as well as self-focusing nonlinearity versus dispersion. It is also demonstrated that the CGLE with different nonlinearities exhibits a rich variety of nonlinear phenomena, including the splitting of the soliton in the initial propagation, the occurrence of breathing of solitons at the beginning of the transmission process, and the formation of multipole solitons. In addition, we discuss that the different propagation regions of the Pearcey–Gaussian beams in the parameter plane of Lévy indexes and dissipative parameters, as well as in the parameter plane of other dissipative parameters. Besides, the required distance before the merger of soliton is mainly affected by the Lévy indexes and the initial amplitudes. Many fascinating and novel phenomena can be observed by reasonably varying dissipative system parameters and input beam parameters. The propagation dynamics of the Pearcey–Gaussian beams can be greatly enriched via the above conclusions and provide the possibility of their application in the field of nonlinear optics.

2 Theoretical model

The propagation of Pearcey–Gaussian beams along axis z in dissipative system can be described by the following cubic–quintic CGLE [30]

$$iu_z - \frac{1}{2}(-\frac{\partial^2}{\partial x^2})^{\frac{\alpha}{2}}u + i\beta(-\frac{\partial^2}{\partial x^2})^{\frac{\alpha}{2}}u + i\delta u + |u|^2 u + i\varepsilon|u|^2 u + v|u|^4 u + i\mu|u|^4 u = 0 \quad (1)$$

The fractional derivative of Eq. (1) is the integral operator that can be defined as

$$\left(-\frac{\partial^2}{\partial x^2}\right)^{\alpha/2} u = \frac{1}{2\pi}\int\int^{d} kd\xi|k|^{\alpha}u(\xi)\exp[ik(x-\xi)] \quad (2)$$

where u is the light field, k is the spatial frequency, x and z are the transverse coordinate and transmission distance respectively. The cubic self-focusing coefficient is equal to 1, and the quintic self-defocusing coefficient is v. α is the Lévy index. The interval of values of α is $1 \le \alpha \le 2$. In fractional quantum mechanics and Lévy path integrals, Lévy index also takes values in this interval [31, 32]. On the one hand, most of the soliton solutions of the fractional nonlinear equations are concentrated in the range where $1 \le \alpha \le 2$ [33], mainly because critical collapse and supercritical collapse occurs when the $\alpha \le 1$. On the other hand, in the limit where the $\alpha = 2$, the fractional Laplace operator is reduced to the classical integer Laplace operator, and then the Eq. (1) naturally reduces to the well-known CGLE.$\beta > 0$ represents dispersion gain, $\delta < 0$ denotes linear loss, $\varepsilon > 0$ is the cubic gain, and $\mu < 0$ accounts for the quintic loss coefficient.

Here, the Pearcey–Gaussian beam is chosen as the input beam

$$\psi(x,0) = APe(x)\exp(-\chi_0^2 x^2) \quad (3)$$

where A is the amplitude of the Pearcey–Gaussian beam and χ_0 is the distribution factor. $Pe(x) = \int_{-\infty}^{+\infty}\exp[i(s^4 + s^2 x)]ds$ is the one-dimensional Pearcey function.

3 Numerically analysis and discussion

By systematic numerical simulations, various results produced may be vividly exhibited for parameter value $v = -0.1$. In simulations, the distribution factor of the input bean $\chi_0 = 0.1$ is fixed. To report results of numerical simulations in detail, firstly, we investigate the influence of the linear loss coefficients and of the Lévy indexes on the optical field propagation. The interesting phenomenon can be easily observed from Fig. 1a, where the different propagation scenarios in the parameter plane of the linear loss coefficient and Lévy index is presented. In region b of Fig. 1a, when the linear loss coefficient is too small to ensure stable propagation of the self-trapped state, and in the case of large linear loss and small Lévy index, stable solitons cannot be produced, the input beam decays during transmission as Fig. 1b show. It is noted that we give a comparison of beams evolution as the

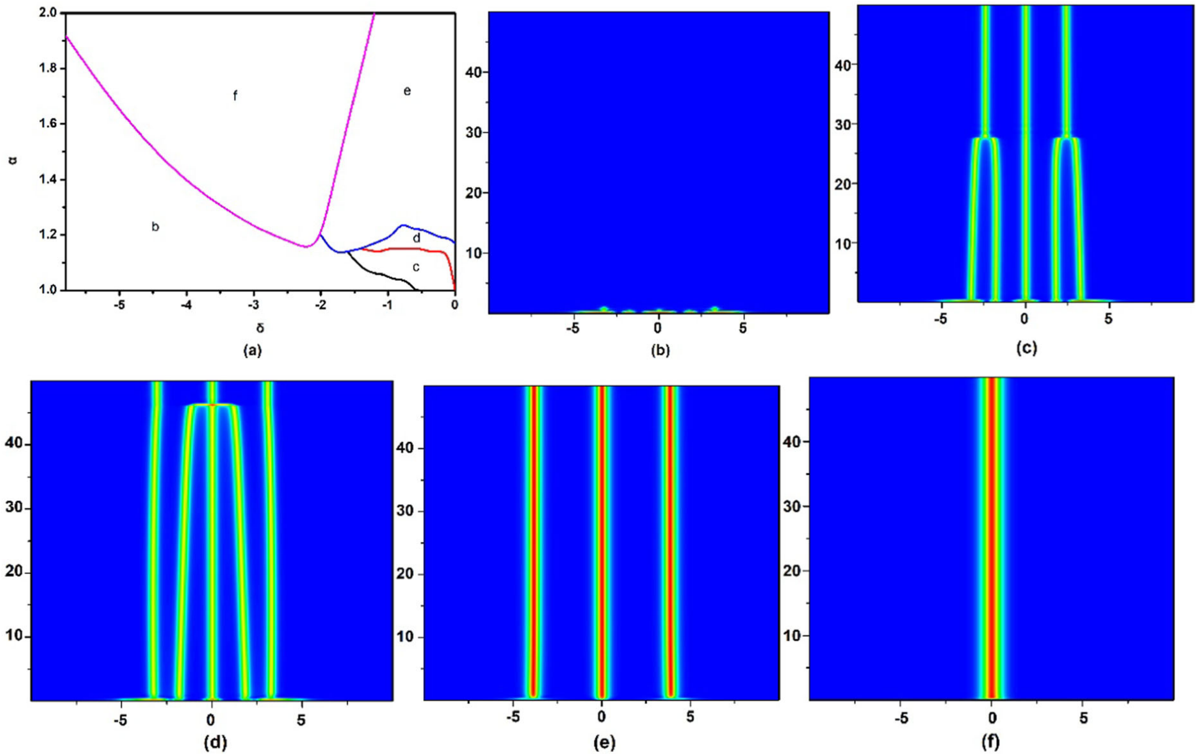

Fig. 1 **a** is the domains of the different propagation scenarios in the plane of parameters (δ, α) of the input Pearcey–Gaussian beam for fixed $\beta = 3, \varepsilon = 2.5, \mu = -0.1$. Region b: decay of the input Pearcey–Gaussian beam; Region c: a tertiary soliton formed by the merger of two solitons; Region d: a tertiary soliton formed by the merger of three solitons; Region e: the input light field evolves into three solitons; Region f: the input light field evolves into one soliton. **b** Dissipation of the input Pearcey–Gaussian beam for $\delta = -1.3, \alpha = 1$ [corresponds to region b shown in Fig (a)]. **c** Formation of tertiary solitons due to the merger of two solitons for $\delta = -0.7, \alpha = 1.1$ [corresponds to region c shown in Fig (a)]. **d** Formation of tertiary solitons because of the merger of three solitons for $\delta = -0.4, \alpha = 1.2$ [corresponds to region d shown in Fig (a)]. **e** Formation of three solitons for $\delta = -1.3, \alpha = 1.5$ [corresponds to region e shown in Fig (a)]. **f** Formation of one soliton $\delta = -3.5, \alpha = 2$ [corresponds to region f shown in Fig (a)]. Here, the other parameters are $A = 3, \chi_0 = 0.1$

region c and region d of Fig. 1a show. When the linear loss coefficients take values between the black line and the red line in Fig. 1a, multipole solitons are generated, and the number of solitons decreases from five to three for the further the transmission distance, and then it keeps transmitting stably with three parallel solitons in Fig. 1c. The phenomenon is mainly attributed to the fact that the two solitons located on both sides of the center position respectively merge into one soliton after the short transmission distance, leading to the formation of three parallel solitons. If the linear loss coefficient takes values in region d in Fig. 1a, the pattern of generated multipole solitons is different from that formed in region c. And the details are presented in Fig. 1d, three solitons in the center position quickly merging into one soliton during transmission, and then three solitons with parallel transmission are formed. For $\delta = -1.4$, the region d vanishes as Fig. 1a show. For further increasing the Lévy index and making the linear loss coefficient take values in the region e in Fig. 1a, the input beam evolves into three solitons as shown in Fig. 1e. Finally, when the linear loss coefficients take values in the region f in Fig. 1a, the input beam transmits stably with single soliton. If we further decrease linear loss coefficient by less than -5.9, the single soliton phenomenon in the region f of Fig. 1a will disappear. These interesting phenomena indicate the complexity

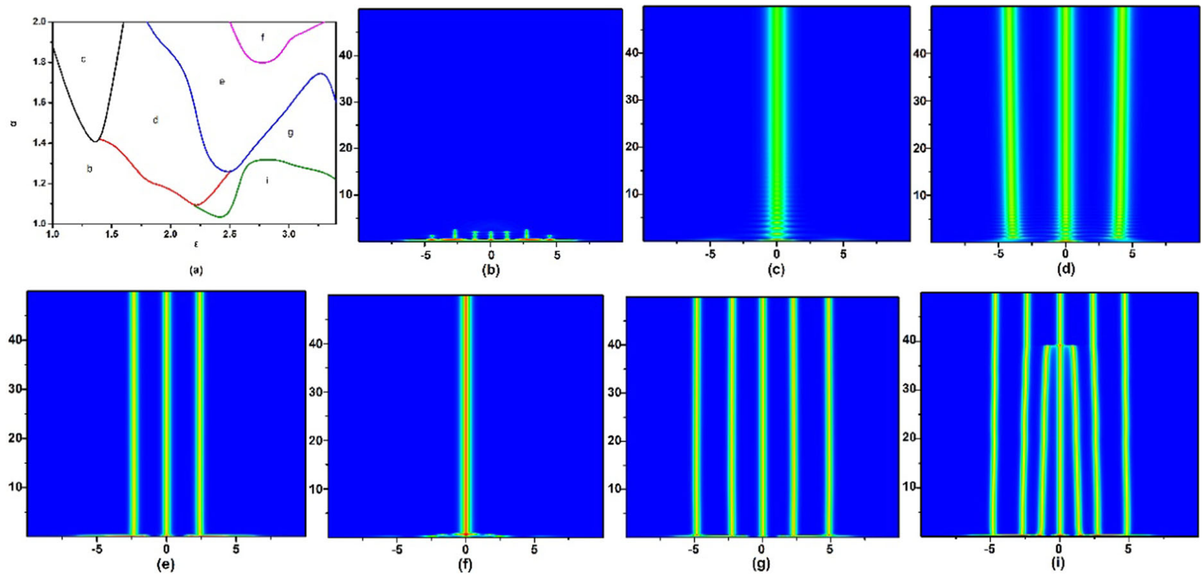

Fig. 2 **a** is the domains of the different propagation scenarios in the plane of parameters (ε, α) of the input Pearcey–Gaussian beam for fixed $\beta = 2$, $\delta = -0.5$, $\mu = -0.1$. Region b: decay of the input Pearcey–Gaussian beam; Region c: the self-capture soliton exhibit breathing phenomenon at the initial propagation; Region d: three solitons exhibit breathing phenomenon at the initial propagation; Region e: the input light field evolves into three solitons; Region f: the input light field evolves into one soliton; Region g: the input light field evolves into multiple solitons; Region i: multiple solitons formed by the merger of three solitons. **b** Dissipation of the input Pearcey–Gaussian beam for $\varepsilon = 2.5, \alpha = 1$ [corresponds to region b shown in Fig (a)]. **c** Formation of a stable soliton with initial breathing states for $\varepsilon = 1.3, \alpha = 1.5$ [corresponds to region c shown in Fig (a)]. **d** Formation of three stable solitons with initial breathing states for $\varepsilon = 1.5, \alpha = 1.5$ [corresponds to region d shown in Fig (a)]. **e** Formation of three stable solitons for $\varepsilon = 2.6, \alpha = 1.4$ [corresponds to region e shown in Fig (a)]. **f** Formation of a stable soliton for $\varepsilon = 2.9, \alpha = 1.8$ [corresponds to region f shown in Fig (a)]. **g** Formation of multiple solitons for $\varepsilon = 2.8, \alpha = 1.4$ [corresponds to region g shown in Fig (a)]. **i** Formation of multiple solitons due to the merger of three solitons for $\varepsilon = 2.7, \alpha = 1.3$ [corresponds to region i shown in Fig (a)]. Here, the other parameters are $A = 3, \chi_0 = 0.1$

of the effects of the linear loss coefficients and the Lévy indexes. According to Fig. 1, we conclude that the formation of the soliton can be controlled by adjusting the values of linear loss and Lévy index.

For obviously depicting beams dynamics, the results summarized in Fig. 2 show that the beam can evolve into seven different outcomes. The different propagation scenarios in the parameter plane of the cubic gain coefficient and Lévy index are given in Fig. 2a. In region b in Fig. 2a, it is found that the input decays under the action of smaller the cubic gain coefficient and larger Lévy index (larger the cubic gain coefficient and smaller Lévy index), which cannot support stable propagation, as shown in Fig. 2b. When the cubic gain coefficients take values in region c in Fig. 2a, the beam shows periodic breathing phenomenon in the initial stage of propagation under the effect of larger Lévy index. However, the periodic breathing property of beams gradually disappears during propagation and eventually a stable soliton-like state occurs, as shown in Fig. 2c. Region c of Fig. 2a disappears at $\varepsilon = 1.6$. When the cubic gain coefficient increases to values in region d of Fig. 2a, the beam has the breathing phenomenon in the initial propagation, which disappears as the propagation distance increases and eventually forms three stable solitons as Fig. 2d show. The input evolves into three stable solitons for further increasing the cubic gain coefficients, and the interval between solitons also becomes smaller as shown in Fig. 2e. In addition, in region f of Fig. 2a, strong diffraction effect leads to the formation of stable single soliton, as shown in Fig. 2f. The input evolves into five mirrored solitons when the cubic gain coefficient takes values in the region g in Fig. 2a, as shown in Fig. 2g. Finally, the influence of weak diffraction phenomenon can be indicated from the region i of Fig. 2a, the pattern of the generated multipole solitons distinctly changes which three solitons in the center position merge into one soliton during propagation, and then it keeps transmitting

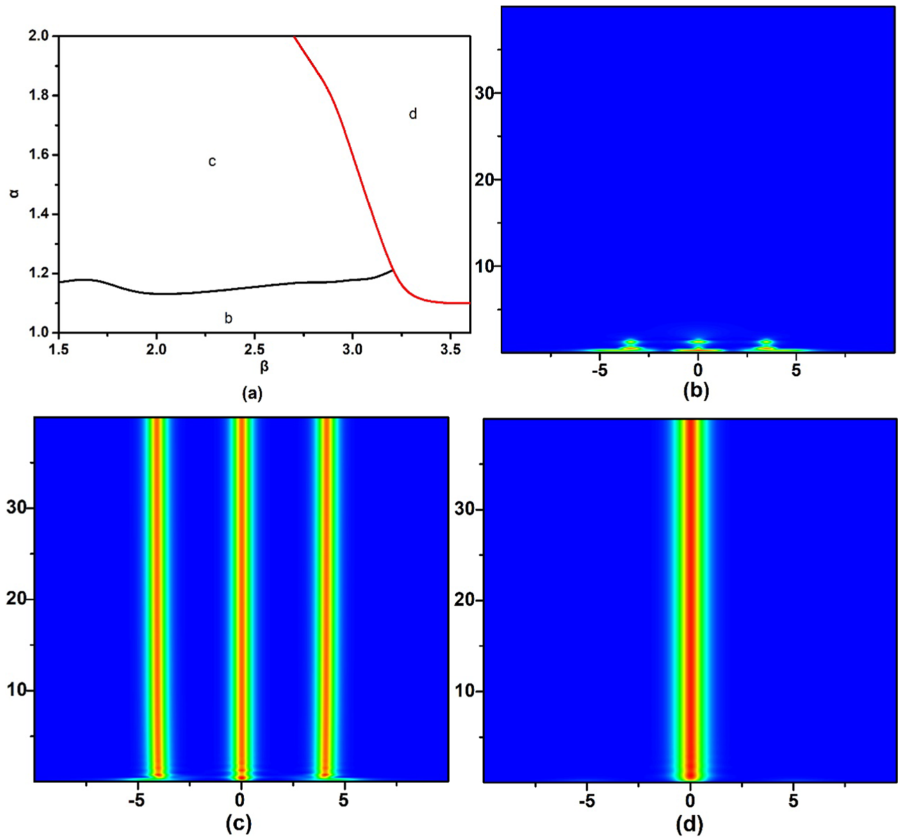

Fig. 3 **a** Domains of different propagation scenarios of the input Pearcey–Gaussian beam in the plane of parameters (β, α) with fixed $\delta = -0.5, \varepsilon = 2, \mu = -0.1$. Region b: decay of the input Pearcey–Gaussian beam; Region c: the input light field evolves into three solitons; Region d: the input light field evolves into a soliton; **b** Dissipation of the input Pearcey–Gaussian beam for $\beta = 2.5, \alpha = 1.1$ [corresponds to region b shown in Fig (a)]. **c** Formation of three stable solitons for $\beta = 2.4, \alpha = 1.6$ [corresponds to region c shown in Fig (a)]. **d** Formation of three stable solitons for $\beta = 3.5, \alpha = 1.8$. Here, the other parameters are $A = 3, \chi_0 = 0.1$

stably in the five solitons state, as Fig. 2i show. One can conclude that the state and the number of dissipative solitons can be changed by choosing the cubic gain coefficient and Lévy index reasonably.

The effect of dispersion gain coefficient and Lévy index on the parameter region of propagation scenarios of symmetrical Pearcey–Gaussian beams is displayed in Fig. 3a. In region b of Fig. 3a, the input decays because of the impact of weak diffraction, as shown in Fig. 3b. It produces three solitons traveling in parallel to each other if we take value of region c in Fig. 3a, as shown in Fig. 3c. And it can be seen from Fig. 3a that the region c will no longer exist if the diffraction gain coefficient is equal to 3.2. When the diffraction gain coefficient takes values in the region d in Fig. 3a, the input beam develops into single soliton state, as shown in Fig. 3d. Therefore, the number of solitons can be controlled by changing the diffraction gain coefficient and the Lévy index.

In order to give an intuitive view to the adjusting effect of the Lévy index, the relationship between the merger distance of two solitons and Lévy index is evidently presented in Fig. 4a. For a deeper understanding of beam dynamics, the evolution of three points on the black line of Fig. 4a is given in Fig. 4b–d, respectively. From Fig. 4b–d, it can be seen that the input forms stable dissipative solitons when the nonlinearity and diffraction, gain and loss are balanced simultaneously. The weak diffraction gain and the strong quintic loss lead to the merging of the two solitons. In particular, it is easy to find in Fig. 4a that the merger distance of two solitons depends on the Lévy index. The merger distance decreases with the increment of the Lévy index, and then tends to be constant. For smaller diffraction gain coefficient, the merger distance becomes the larger as the black line in Fig. 4a display, however, while the larger absolute value of quintic loss coefficient makes the merger distance smaller, as shown in the pink line in Fig. 4a. Comparing the red line and blue line in Fig. 4a, it can be found that the effect of varying the linear loss coefficient on the merge distance is basically

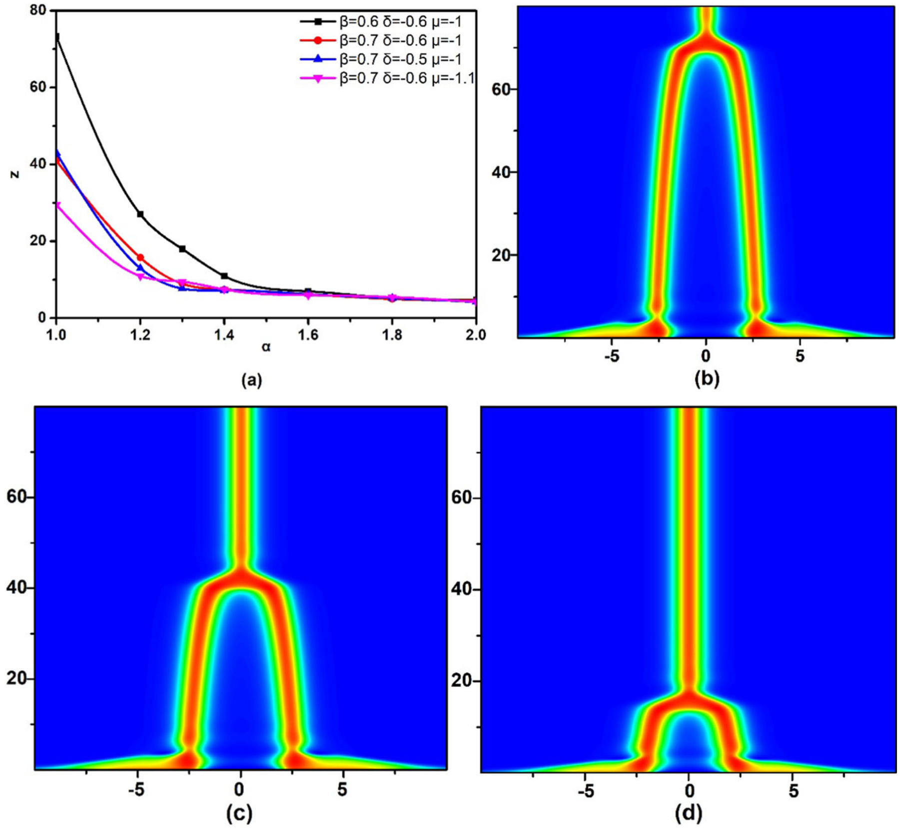

Fig. 4 **a** The transmission distance necessary for two stable solitons to merge as a function of Lévy indexes. For fixed $\beta = 0.6, \delta = -0.6, \mu = -1$, examples of the merger when we take different Lévy indexes **b** $\alpha = 1$ **c** $\alpha = 1.1$ **d** $\alpha = 1.3$. Here, the other parameters are $A = 3, \chi_0 = 0.1, \varepsilon = 2.5$. (Color figure online)

invariant. Therefore, it is possible to control the required transmission distance before the two solitons merger by appropriately changing the value of the Lévy index.

The initial pulse amplitude represents the significant influence on dynamics of the generated soliton. Figure 5a shows the required transmission distance before the merger of the three solitons versus the initial amplitude. The evolution of three points taken on the black line in Fig. 5a can be indicated from Fig. 5b–d. Note that the merger distance apparently increases with the initial amplitude. As shown in the black and red lines in Fig. 5a, it is interesting to verify the fact that for fixed the initial amplitude, the merger distance of the three solitons increases obviously with the decrease of the diffraction gain coefficient. It can be seen from the red line and blue line in Fig. 5a, the smaller the absolute value of linear loss coefficient leads to the merger distance larger. As a result, the conclusion can be obtained with no difficulty that the merger distance of the three solitons is controlled by changing the value of the initial amplitude, linear loss coefficient and diffraction gain coefficient. Thus, evolution state of multipole solitons can be controlled.

The influence of the cubic gain coefficient and linear loss coefficient on the optical field propagation can be observed from Fig. 6a, where different propagation scenarios in the parameter plane of the cubic gain coefficient and linear loss coefficient is given. When the cubic gain coefficient takes values in region b in Fig. 6a, the input rapidly decays because the cubic gain coefficient is too small, and the phenomenon can be explained that the external gain cannot balance the strong loss, as shown in Fig. 6b. The input Pearcey–Gaussian beam starts to evolve into stable single soliton when the cubic gain coefficient increases to values in region c of Fig. 6a, as shown in Fig. 6c. If the cubic gain coefficient is further increased, it causes the expansion phenomenon of the input beam due to excess gain, as shown in Fig. 6d. In Fig. 6a, there is the similar propagation scenario is presented in the parameter plane of the cubic gain coefficient and the diffraction gain coefficient. It can be concluded that the cubic gain coefficient is an important factor

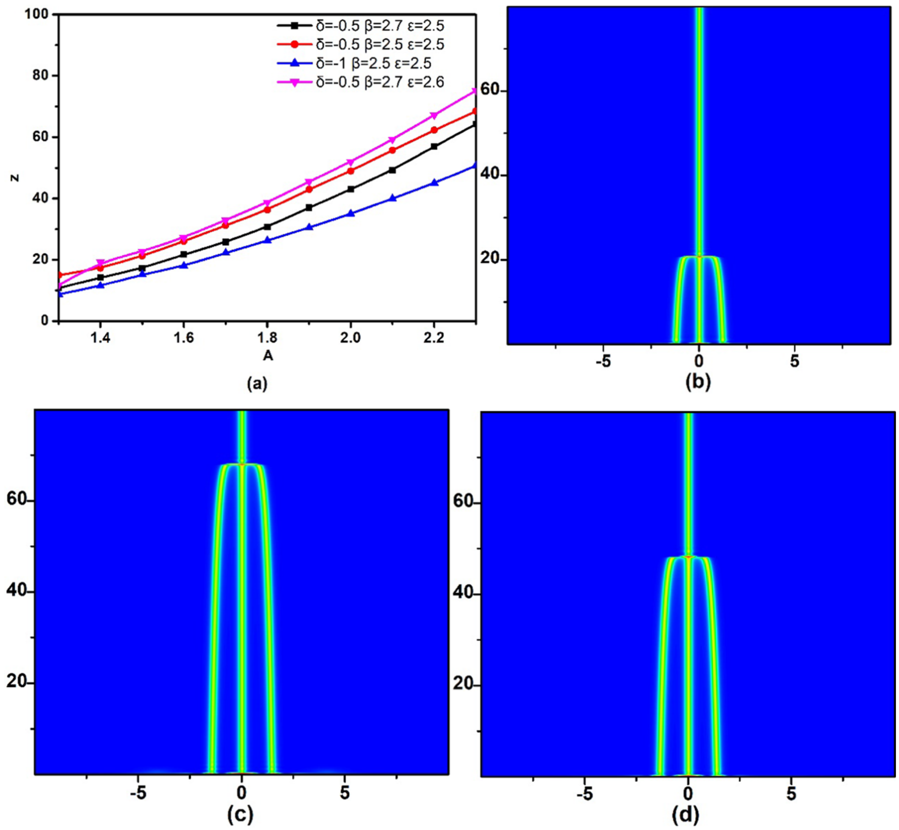

Fig. 5 **a** The transmission distance necessary for three stable solitons to merge as a function of initial amplitudes. For fixed $\delta = -0.5, \beta = 2.5, \varepsilon = 2.5$, examples of the merger when we take different initial amplitudes **b** $A = 1.5$ **c** $A = 2$ **d** $A = 2.3$. Here, the other parameters are $\chi_0 = 0.1, \alpha = 1.1, \mu = -0.1$. (Color figure online)

affecting the formation of stable single soliton, too small will lead to diffraction, but too large will also make the beam spread.

To understand the influence of the quintic loss coefficient on the evolution of the generated solitons, the evolution of Pearcey–Gaussian beams for different values of the Lévy index and quintic loss coefficient is showed in Fig. 7. It can be seen from Fig. 7 that the input beam forms single soliton, multipole solitons and other soliton-like states resulting from the joint balance of self-focusing nonlinearity and diffraction, gain and loss. In Fig. 7a1, the mirrored multipole solitons are generated during propagation, as the Lévy index increases, it develops into three parallel-transmitting solitons as Fig. 7b1 show. Further increasing the Lévy index, one can find that two attracting solitons are occurred on both sides of the center position in the initial stage of propagation. But this phenomenon will not exist if the propagation continues, and then the formation of three parallel-transmitting solitons, as shown in Fig. 7c1. In Fig. 7a2–a3, b2–b3 and c2–c3, when $\mu = -0.5$, as the Lévy index increases, the speed at which the beam returns to single soliton becomes faster and faster in the initial stage of propagation. With the increase of the absolute value of the quintic loss coefficient, note that the transverse width of the soliton increases for a larger $|\mu|$.

The evolution of the Pearcey–Gaussian beam for different the cubic gain coefficients and quintic loss coefficients is presented in Fig. 8. As shown in Fig. 8a1–c1, one importance is noted that the generation of multipole solitons. As the cubic gain coefficient increases, the beam evolves into from three parallel solitons to the five parallel solitons. In Fig. 8a2–a3, b2–b3 and c2–c3, the single soliton is formed during transmission when the absolute value of the quintic loss coefficient becomes larger. And the

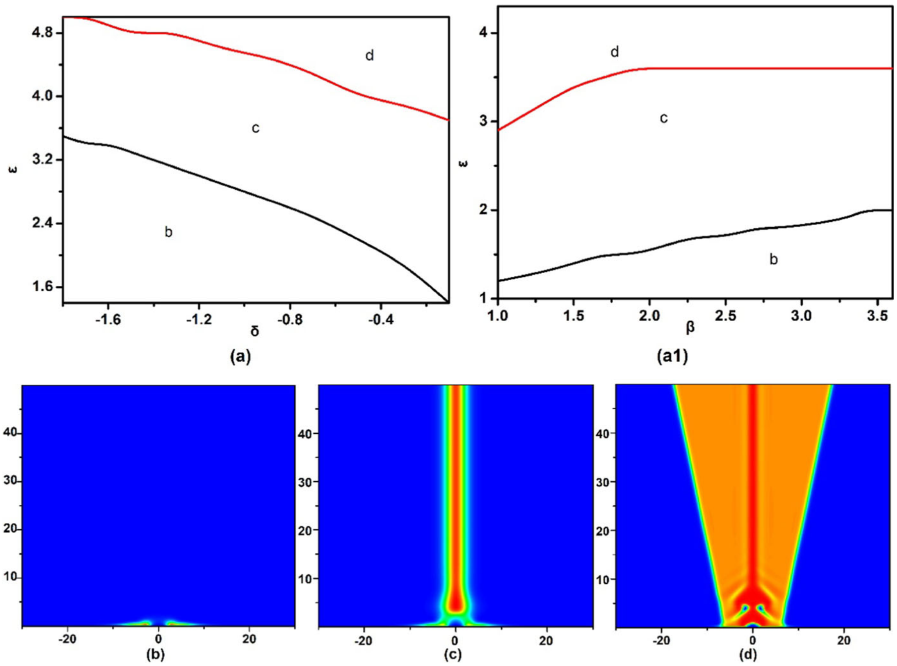

Fig. 6 **a** Domains of different propagation scenarios of the input Pearcey–Gaussian beam in the plane of parameters (δ, ε) with fixed $\beta = 1.6$. **a1** Domains of different propagation scenarios of the input Pearcey–Gaussian beam in the plane of parameters (β, ε) with fixed $\delta = -0.1$. Region b: decay of the input Pearcey–Gaussian beam; Region c: the input light field evolves into a stable soliton; Region d: spread for the underdamped setting; **b** Dissipation of the input Pearcey–Gaussian beam for $\delta = -1.2, \varepsilon = 2.4$ [corresponds to region b shown in Fig (a)]. **c** Formation of stable solitons for $\delta = -0.4, \varepsilon = 2.1$ [corresponds to region c shown in Fig (a)]. **d** Spread for the underdamped setting for $\delta = -1.2, \varepsilon = 4.7$. Here, the other parameters are $A = 3, \chi_0 = 0.1, \alpha = 1.5, \mu = -1$

transverse width of the single soliton is wider with the increase of $|\mu|$. Simultaneously, with the increase of the cubic gain coefficients, the distance which the beam returns to single soliton becomes farther and farther in the initial stage of propagation. Therefore, the reasonable adjustment of the cubic gain coefficient and quintic loss coefficient enables generation of multipole solitons.

4 Conclusion

In summary, the influence of the dissipative coefficient, Lévy index and initial amplitude on the propagation characteristics of Pearcey–Gaussian beams in the complex fractional cubic–quintic Ginzburg–Landau systems is numerically investigated. The systematic simulations evidently reveal the generation of stable multipole solitons and single soliton, in addition to soliton-like. We clearly find that the domains that support the different outcomes of the evolution in various parameter spaces. The effect of the dissipative coefficient and Lévy index on stability regions of dissipative solitons generated is mainly studied. The results show that the pattern of multipole solitons, the number and state of solitons can be controlled by adjusting the dissipative coefficient and Lévy index. In particular, it is demonstrated that the evolution can lead to three different outcomes through the interaction of linear loss or diffraction gain and cubic gain: decay, develop into stable single soliton, expands into the spreading pattern. Besides, the quintic loss shows the significant influence on dynamics of the generated solitons. It is worth mentioning that two solitons or three solitons merge into the single soliton, with the merger distance also determined by Lévy index and the initial amplitude of the input beam. The obtained results provide some realizations and applications in the light guiding and switching.

From the application aspect, the number and position of solitons are controlled by changing parameters of beam and medium in this paper. The

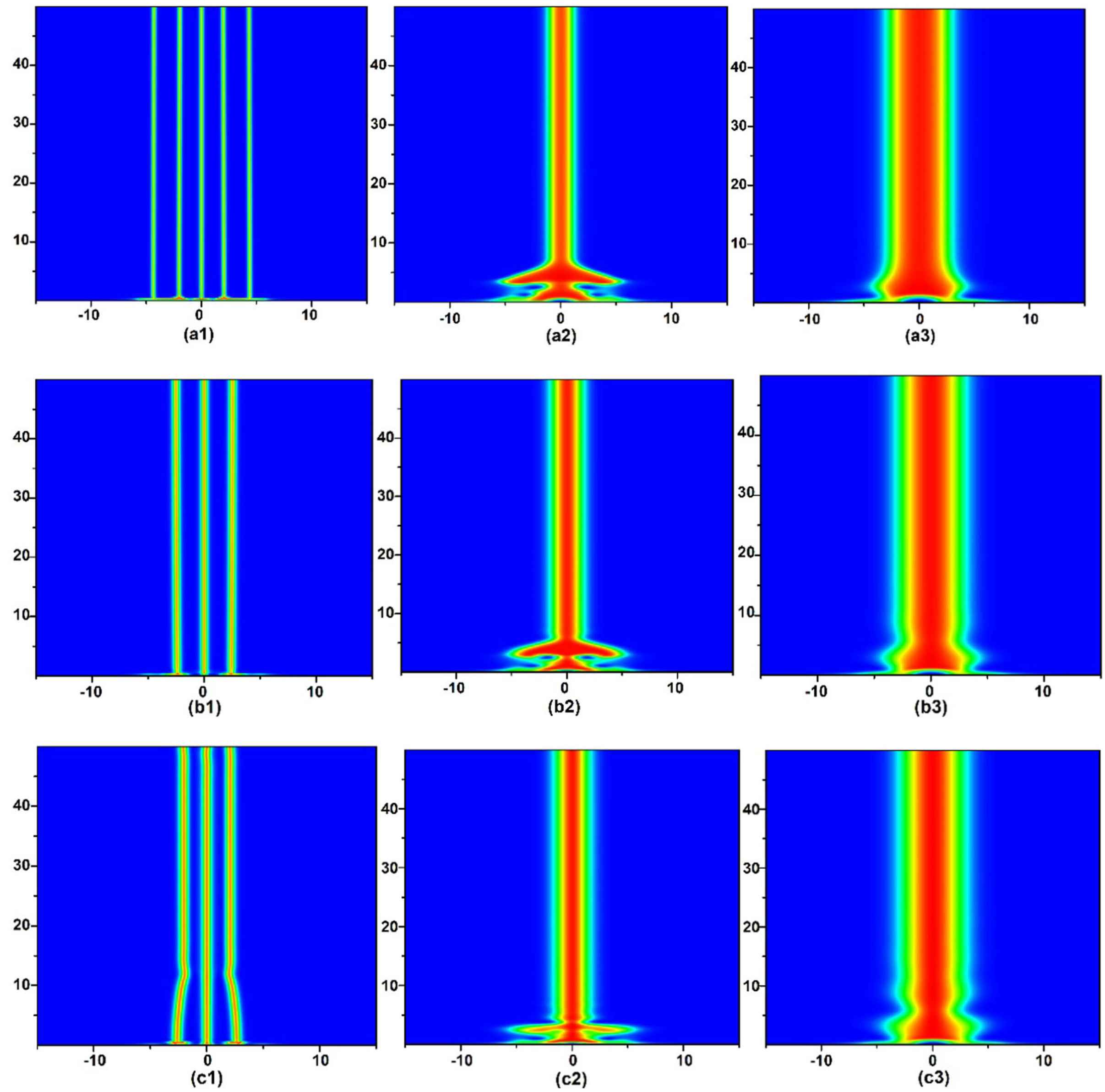

Fig. 7 The evolution of the Pearcey–Gaussian for different Lévy indexes α and quantic loss coefficients μ. The Lévy indexes are respectively $\alpha = 1.2, 1.7, 2$ from top to bottom. The quantic loss coefficients are $\mu = -0.1, -0.5, -1$ from left to right. Here, the other parameters are $A = 3, \chi_0 = 0.1, \beta = 2, \delta = -0.1, \varepsilon = 2.5$

stabilized multipole optical solitons obtained can lay a theoretical foundation for the development of better optical switches, which can provide ideas for the development of new optical switching devices. Simultaneously, the Ginzburg Landau model used in this paper is an important class of nonlinear systems, which describes the existence of many rich physical phenomena in the dissipative medium system, and the optical soliton phenomenon is one of them, so it has a good application value in the fields of optical information processing devices, optical tweezers micro-nano control technology, condensed matter physics, and plasma, etc., especially for the research and development of new optical devices to provide an important theoretical basis.

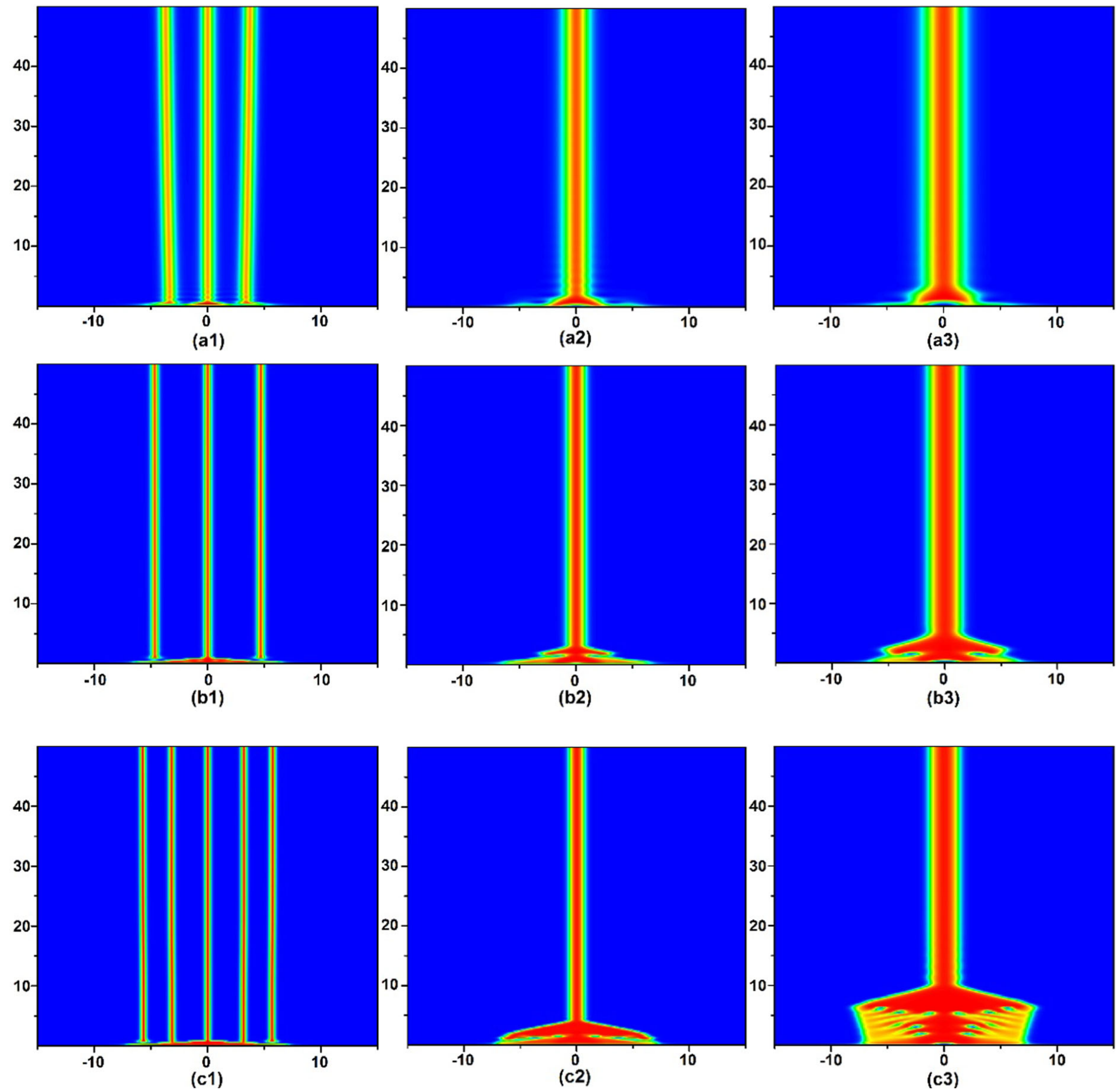

Fig. 8 The evolution of the Pearcey–Gaussian for different cubic-gain coefficients ε and quantic-loss coefficients μ. The cubic-gain coefficients are respectively $\varepsilon = 2, 3.4, 4.4$ from top to bottom. The quantic-loss coefficients are $\mu = -0.2, -0.4, -0.6$ from left to right. Here, the other parameters are $A = 3, \chi_0 = 0.1, \beta = 2, \delta = -0.1, \alpha = 1.4$

Funding The authors have not disclosed any funding.

Data availability Our manuscript has no associated data.

Declarations

Conflict of interest The authors have no relevant financial or non-financial interests to disclose.

References

1. Wang, S.B., Ma, G.L., Zhang, X., Zhu, D.Y.: Study on the regulation of amplitude for the optical soliton through nonlinear effects in the optical communication system. Optik – Int. J. Light Electron Opt. **269**, 169839 (2022)
2. Wang, S.B., Zhang, X., Ma, G.: All-optical switches based on three-soliton inelastic interaction and its application in optical communication systems. Chin. Phys. B **32**, 030506 (2023)

3. Hasegawa, A., Tappert, F.: Transmission of stationary nonlinear optical pulses in dispersive dielectric fibers. I. Anomalous dispersion. Appl. Phys. Lett. **23**, 142–144 (1973)
4. Mollenauer, L.F., et al.: Experimental observation of picosecond pulse narrowing and solitons in optical fibers. Phys. Rev. Lett. **45**, 1095–1098 (1980)
5. Glansdorff, P., Prigogine, I.: Thermodynamic theory of structure: stability and fluctuations. Am. J. Phys. **41**, 147–148 (1971)
6. Feynman, R.P., Vernon, F.L.: The theory of a general quantum system interacting with a linear dissipative system. Ann. Phys. **281**, 547–607 (2000)
7. Soto-Crespo, J.M., Akhmediev, N., Chiang, K.S.: Simultaneous existence of a multiplicity of stable and unstable solitons in dissipative systems. Phys. Lett. A **291**, 115–123 (2001)
8. Liu, B., Liu, Y.F., He, X.D.: Impact of phase on collision between vortex solitons in three-dimensional cubic–quintic complex Ginzburg–Landau equation. Opt. Express **22**, 26203–26211 (2014)
9. Descalzi, O., Cartes, C., Brand, H.R.: Interaction of dissipative solitons stabilized by nonlinear gradient terms. Phys. Rev. E **103**, 042215 (2021)
10. He, J.Y., Wang, P., He, R.J., Liu, C.C., Zhou, M.J., Liu, Y.G., Yue, Y., Liu, B., Xing, D.K., Zhu, K.Y.: Elastic and inelastic collision dynamics between soliton molecules and a single soliton. Opt. Express **30**, 14218–14231 (2022)
11. Rosanov, N.N.: Spatial Hysteresis and Optical Patterns. Springer, Berlin Heidelberg (2002)
12. Malomed, B.A.: Complex Ginzburg–Landau Equation in Encyclopedia of Nonlinear Science. In: Scott, A. (ed.) Routledge (2005)
13. Hong, W.P.: Effect of the random field on the dynamics of pulsating, erupting, and creeping solitons in the cubic–quintic complex Ginzburg–Landau equation. Z. Naturforschung Sect. A-A J. Phys. Sci. **61**, 615–623 (2006)
14. Mejia-Cortes, C., Soto-Crespo, J.M., Vicencio, R.A., Molina, M.I.: Bound states and interactions of vortex solitons in the discrete Ginzburg–Landau equation. Phys. Rev. A **86**, 023834 (2012)
15. He, Y.J., Mihalache, D.: Rotary dissipative spatial solitons in cylindrical lattices. J. Opt. Soc. Am. B **30**, 3135–3139 (2013)
16. He, R.J., Wang, Z., Liu, Y.G., Wang, Z.H., Liang, H., Han, S.M., He, J.Y.: Dynamic evolution of pulsating solitons in a dissipative system with the gain saturation effect. Opt. Express **26**, 33116–33128 (2018)
17. Tarasov, V.E., Zaslavsky, G.M.: Fractional Ginzburg–Landau equation for fractal media. Phys. A **354**, 249–261 (2005)
18. Tarasov, V.E., Zaslavsky, G.M.: Fractional dynamics of coupled oscillators with long-range interaction. Chaos Soliton Fract. **16**, 023110 (2006)
19. Mvogo, A., Tambue, A., Ben-Bolie, G.H., Kofané, T.C.: Localized numerical impulse solutions in diffuse neural networks modeled by the complex fractional Ginzburg–Landau equation. Commun. Nonlinear Sci. **39**, 396–410 (2016)
20. Tasbozan, O.: New optical solutions of complex Ginzburg–Landau equation arising in semiconductor lasers. Appl. Phys. B **125**, 104 (2019)
21. Lu, P.H., Wang, B.H., Dai, C.Q.: Fractional traveling wave solutions of the (2 + 1)-dimensional fractional complex Ginzburg–Landau equation via two methods. Math. Meth. Appl. **43**, 8518–8526 (2020)
22. Huang, C., Li, Z.: New exact solutions of the fractional complex Ginzburg–Landau equation. Hindawi Math. Probl. Eng. **2021**, 6640086 (2021)
23. Abdulkadir, S.T., Mehmet, B.H., Hasan, B.: Optical solitons and other solutions to the conformable space-time fractional complex Ginzburg–Landau equation under Kerr law nonlinearity. Pramana **91**, 58–65 (2018)
24. Arshed, S.: Soliton solutions of fractional complex Ginzburg–Landau equation with Kerr Law and non-Kerr law media. Optik-Int. J. Light Electron Opt. **160**, 322–332 (2018)
25. Fang, J.J., Mou, D.S., Wang, Y.Y., Zhang, C.H., Dai, C.Q., Chen, Y.X.: Soliton dynamics based on exact solutions of conformable fractional discrete complex cubic Ginzburg–Landau equation. Res. Phys. **20**, 103710 (2021)
26. Wang, L.Y.: Exact solutions to the fractional complex Ginzburg–Landau equation with time-dependent coefficients under quadratic–cubic and power law nonlinearities. Nonlinear Dyn. **111**, 4709–4722 (2023)
27. Zhang, L.P., He, S.L., Peng, X., Huang, L.Q., He, Y.J., Deng, D.M.: Tightly focusing evolution of the auto-focusing linear polarized circular Pearcey Gaussian vortex beams. Chaos Soliton Fract. **143**, 110608 (2021)
28. Zhang, S., Zang, F., Dong, L.J., Li, L.: The evolution and interaction of the asymmetric Pearcey–Gaussian beam in nonlinear Kerr medium. Appl. Phys. B **128**, 179 (2022)
29. Wu, J.W., Cai, H.Y., Yu, P.X., Gong, P.R., Man, Z.S., Deng, D.M., Zhang, L.P.: The multi-consecutive optical bottles generated from the chirped elliptical Pearcey Gaussian vortex beams. Res. Phys. **39**, 105747 (2022)
30. Qiu, Y.L., Malomed, B.A., Mihalache, D., Zhu, X., Zhang, L., He, Y.J.: Soliton dynamics in a fractional complex Ginzburg–Landau model. Chaos Soliton Fract. **131**, 109471 (2020)
31. Laskin, N.: Fractional quantum mechanics. Phys. Rev. E **62**, 3135–3145 (2000)
32. Longhi, S.: Fractional Schrödinger equation in optics. Opt. Lett. **40**, 1117–1121 (2015)
33. Aldushin, A.P., Malomed, B.A.: Phenomenological theory of spin combustion. Combust. Flame **42**, 1–6 (1981)